Bosonic lasing and trapping of a dressed photon fluid in InGaN at room temperature

Munise Cobet*

Institute of Condensed Matter Physics, École Polytechnique Fédérale de Lausanne, 1015 Lausanne, Switzerland

(Received 30 June 2015; revised manuscript received 7 July 2016; published 4 August 2016)

The generation of a quantum fluid of dressed photons at room temperature is experimentally demonstrated in an InGaN microcavity which is divided into two- and one-dimensional sections, resulting in single- and switchable multilevel coherent light emission. Ultra-low-threshold operation is attributed to the slight but robust excitonic fraction of the photonic condensate representing a bosonic laser working below the Mott transition (polariton laser). In contrast to equilibrium Bose-Einstein condensates, the nonequilibrium driven-dissipative nature enables the population of higher orbitals if any confinement potential is present to induce enhanced quantum correlations. Trapping inside microwire spacers leads to a polariton harmonic oscillator resulting in discrete states in an equidistant ladder of photonic orbitals. Level occupation and selection of a specific wave function is managed via optical control, mimicking a quantum emitter on a macroscopic level. It shows that exotic states of matter can be realized in rather simple structures at room temperature directly visible to the human eye. It represents also an excellent opportunity to study basic many-body dynamics in one-dimensional bosonic matter by simultaneously settling an optimized fabrication technique for devices enabling practical Boolean quantum logic gates for optical computing.

DOI: 10.1103/PhysRevB.94.075302

I. INTRODUCTION

Measuring collective quantum effects in a many-body ensemble of interacting photons at optical frequencies is a long-desired goal but it is challenging since light basically propagates linearly without any intercorrelation. To redefine the effective interaction between photons, a nonlinear medium [1,2] or the giant modulation in the optical response (dielectric function) of a medium containing excitons with a high oscillator strength [3–5] can be used. The quantification of eigenmodes of a radiation field near excitonic resonances leads to new mixed light-matter quasiparticles of *dressed photons* also known as *polaritons*.

Conventional semiconductor lasers, e. g., vertical cavity surface emitting lasers (VCSELs), commonly use an electron-hole plasma in an optical microcavity (MC) to launch the stimulated light emission (lasing) once the regime right above the Mott transition (similar to the Bernard-Durraffourg condition) is exceeded and bosonic excitons turn fermionic. Contrary to this conventional fermionic laser, a bosonic laser where excitons are still stable can be basically established in the very same device structure. It was proposed by Imamoğlu *et al.* [6] that photoexcited Bose-Einstein condensates [7] formed in such a MC would represent a laserlike device able to operate completely without population inversion and therefore theoretically with a zero-threshold driving power by utilizing the above-mentioned many-body coherences. The partly misleading term "population inversion" (i. e., having more electrons in the conduction band than in the valence band), which is commonly used to describe lasing in solid-state systems, and using instead the Bernard-Durraffourg condition for the case of semiconductors has been already discussed [8]. The spontaneous radiative decay in the form of nonlinear coherent light emission prevents the condensate from getting fully thermalized. Photonic quantum fluids can exist at elevated temperatures due to the small effective mass leading to large de Broglie wavelengths. Hence, trapping can be realized simply by micrometer-sized structures. In reducing the motional degree of freedom, stronger quantum correlations are the consequence. In analogy to quantum boxes, standing waves with excited energies at finite wave numbers occur as the center-of-mass position is fixed and the system can populate higher orbitals [9], resulting in a coherent multilevel condensate. In the case of a one-dimensional (1D) harmonic trap, the result is a "harmonic fluid" [10] and the quantization into levels with equal energy spacing. For condensed quasiparticles being in the same quantum state, the phase of the system is defined as for a single particle and coherence is given on macroscopic scales, described by one many-body wave function Ψ. For decaying polariton condensates the amplitude of probability, $|\Psi|^2$, can be directly observed via its emission spectrum.

In this article, the generation of photoexcited singular and multilevel Bose condensates of exciton polaritons with a very high photonic fraction [11,12] (dressed photons) at room temperature (RT) with ultralow threshold in an InGaN/GaN MC is reported. Collective modes of harmonic motion within micrometer-sized traps are observed by imaging $|\Psi|^2$ in momentum and real space. The spectrum of this multimode polariton laser is theoretically reproduced using the Gross-Pitaevskii equation accounting for the nonlinear harmonic oscillation.

II. EXPERIMENT

Since the first observation of polariton Bose condensation [7], it has not been convincingly observed in InGaN. But, InGaN is the most important material of present and future solid-state lighting. No other semiconductor has exhibited such success in the past decade. White light-emitting diodes (LEDs) and blue lasers (Blu-Ray) made from InGaN are having an enormous impact on society, environment, and science. In contrast to GaN and ZnO, better electrical carrier injection through *p* contacts and visible light emission is given by using InGaN.

*Present address: Faculty of Engineering and Natural Sciences, Johannes Kepler University, Linz, Austria; munise.cobet@alumni.tu-berlin.de

To date, polariton lasing at RT was achieved in structures and materials, which are far away from being practical or easy to fabricate. For GaN and ZnO, which indeed fulfill the condition of stable excitons at RT, polariton condensation was made possible by using bulk active medium [12,13] or a very large number of quantum wells (QWs) [14] to maintain efficient coupling, or in exotic structures like single nanowires [15]. The only electrical pumped device [16] needs a very special and complicated processing. Promoting well-established InGaN VCSEL structures to be suitable for polariton condensation is the strategy of choice and the missing building block towards a practical quantum device able to operate at RT and in the strongly demanded visible (blue) wavelength and provides an elegant way to reduce the power consumption to an unbeatable minimum [17].

Several attempts have been made to achieve polariton condensation in InGaN but the impact of the inhomogeneous broadening due to composition and thickness fluctuations is the most challenging issue in these layers. Placed in a resonator with either a large effective cavity length or low finesse, the coupling is not effective enough. But instead of increasing the number of QWs to maximize the coupling strength, the main effort here focused on reducing the effective cavity length which in turn would compensate for a lower number of QWs, an essential qualification for electrically driven devices. The most promising solution to reduce the cavity length L_{eff} and provide high finesse is therefore the use of a double dielectric mirror, i.e., the full hybrid approach. This path is advantageous because of the close analogies to the well-established VCSEL design, while the fabrication is possible by using mainly standard chip processing techniques [see Fig. 1(a)]. The cavity active zone must be grown on a lattice-matched template to achieve a high quality and narrow excitonic linewidths. Consequently, the use of two dielectric distributed Bragg reflectors (DBRs) to form a MC requires the liftoff of the active region. The preservation of quality during the processing with (electro)chemical and mechanical treatment has shown to be the most important step for a successfully operating device.

The 4λ cavity consists of five sets of three $In_{0.1}Ga_{0.9}N/GaN$ QWs (2/3 nm) sandwiched between dielectric (DBRs) and is schematically drawn in Fig. 1(a). With $L_{\text{eff}} = 954$ nm, the full hybrid (double dielectric) sample is more than 4.5 times shorter than the semihybrid microcavity [14], where L_{eff} is 4356 nm. This property is seen as the key feature that enables polariton formation in InGaN in contrast to the different previous structures. Please see the Supplemental Material for details of the sample design [18].

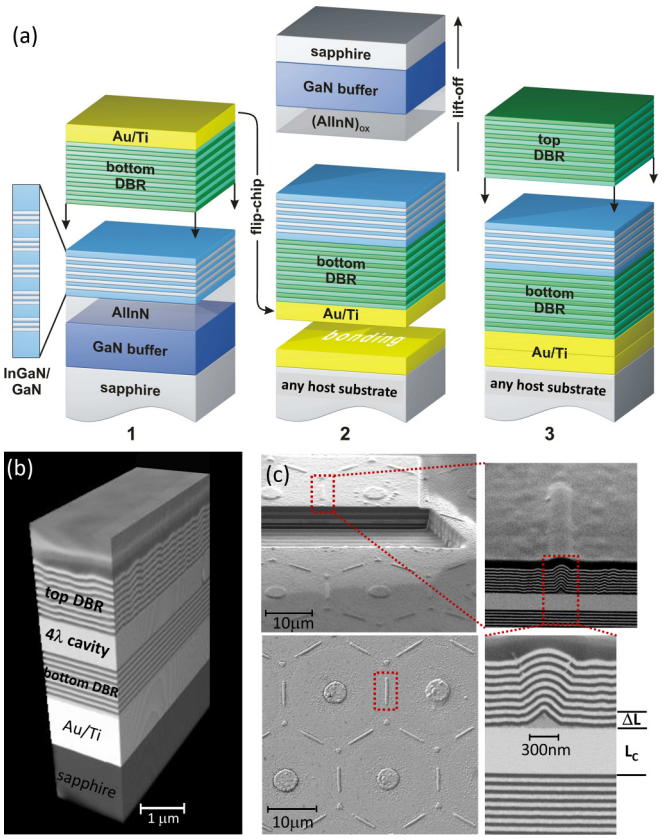

FIG. 1. Sample design and structural properties of the double dielectric microcavity with InGaN active medium. (a) Main fabrication steps for the two-dimensional (2D) cavity: (1) growth on lattice matched template and deposition of bottom DBR, (2) flip-chip bonding onto any gold-coated host substrate and sacrificial layer removal, and (3) deposition of top DBR. Focused ion beam-prepared 3D SEM tomography of (b) the 2D region and (c) of the microstructured region showing the spacer profile of the traps.

A. Fabrication

The fabrication begins with the growth of the multilayer structure by metal organic vapor phase epitaxy (MOVPE) on a 2-in. *c*-plane sapphire substrate. After a 3-μm-thick GaN buffer, a lattice-matched 200-nm-thick $Al_{0.83}In_{0.17}N$ layer is grown. The structure is then completed by a 15-period $In_{0.1}Ga_{0.9}N$ (2 nm)/GaN (3 nm) multi-quantum-well 3λ cavity between two 82-nm GaN spacers (overall 4λ). After the growth, SiO_2 is deposited. Standard UV photolithography is used to create mesas of different diameters (from 60 to 300 μm). The sample is then etched using inductively coupled Cl_2/Ar plasma to give access to the AlInN layer sidewalls. Lateral electrochemical oxidation of the AlInN sacrificial layer is done in a NTA:KOH solution of 11 pH at 0.1 kA/cm^2 [19,20]. By appropriate oxidation stop, residual transparent walls of unoxidized $Al_{0.83}In_{0.17}N$ allow one to engineer a cavity-spacer micropattern on top of the GaN which can be used for the photonic traps. The SiO_2 hard mask is kept until the end of this process to protect the top GaN surface. The deposition of an eight-pair bottom dielectric SiO_2/ZrO_2 DBR by e-beam evaporation proceeded after the removal of the SiO_2 mask in a buffered fluoridric acid solution. Ti/Au metallization is used on the top of the bottom DBR as well as on another host sapphire substrate (any other host material can be used as long it has a suitable smooth Au surface for the bonding). Another major step consists in the thermocompression bonding process between the Au layers of the sample and the new host substrate in a homebuilt bonding machine in a vacuum environment (1×10^{-5} mbar) at 320°C for several hours.

The removal of the $(AlInN)_{ox}$ and the sapphire substrate is done in a nitric acid solution with a dilution ratio of 32% heated to 100°C by lateral etching of the AlInN sacrificial layer with a rate of 2μm/h, keeping the microtrap wires and

dots on the surface. Finally, the microcavity is completed by the deposition of an eight-pair top dielectric SiO_2/ZrO_2 DBR by e-beam evaporation.

B. Optical and structural properties

The measured quality factor of the final chip averaged over an area of 100 μm^2 is $Q = 850$ in the unstructured region. The thickness fluctuations of the top DBR are seen as the main source of the photonic broadening. Inside any confinement potential, the local Q is assumed to be considerably larger. The measured stop-band width is 95 nm (745 meV) centered around 3.0 eV with a reflectivity of 99.3%.

Scanning electron microscopy (SEM) shows the hexagonal pattern of spacers with wire- and dotlike geometry and is displayed in Fig. 1(c). The wirelike structures have a length of $l = 6\ \mu m$, a bottom width $w = 350$ nm, and a cavity thickness difference of $\Delta L \approx 200$ nm. Hence it is considered that the motional degrees of freedom for particles with a wavelength $\lambda_{dB}/2 \geqslant 350$ nm inside the wire traps are truly reduced to one dimension. As long the propagation in this direction is still shorter than the coherence length of the condensate, it will get fully quantized by forming a standing wave with discrete levels. Figures 1(b) and 1(c) show the tomographic SEM cross section for the unstructured area as well as the spacer traps, respectively. In contrast to steps in the cavity thickness [21] that cause sharp discontinuities in the photonic defect band, smooth triangular spacer shapes [Fig. 1(c)] reduce scattering losses [22] leading to a higher quality factor.

The dispersion can be scanned directly by angle-resolved optical techniques because the emission of leakage photons happens under k conservation. Measurement techniques are Fourier and real-space imaging to record all the information of the particular eigenstates. A microscope objective with a numerical aperture of 0.55 is used to image the far-field photoluminescence (PL) on a cooled CCD chip mounted to a monochromator in order to probe the spectral and angular evolution of the eigenmodes under optical pumping. The frequency-quadrupled laser line (266 nm) of a Nd:YAG laser with a repetition rate of 8.52 kHz and a pulse duration of 500 ps (quasicontinuous wave) is used as a pump source to inject incoherent carriers above the band edge of GaN. The diameter of the excitation spot is 8 μm. Fourier images are taken for different temperatures and swept pump powers.

Tuning photonic and excitonic modes independently of each other enables creation of quasiparticles with different excitonic fractions given by the Hopfield coefficient. Large negative detuning is characterized by a high photonic fraction [11] and forms deeper traps and reduces thermal escape, a relevant condition for RT. To turn out the very large photonic fraction, the notation of "dressed photons" is used rather than "polaritons."

Stochastic conversion between stable excitons and light can be sufficient for an effective stimulation mechanism [23] if the inflow of bosons to the final state is exceeding the dissipative losses (spontaneous symmetry breaking).

III. RESULTS AND DISCUSSION

A PL peak analysis of the bare exciton yields values for the inhomogeneous broadening of $\sigma = 40$ meV. Transfer-matrix simulations show that clear normal mode splitting, where the conversion of excitons and photons turns coherent, reshaping the dispersion curves into the nonperturbation regime, is around 41 meV for the studied sample [18].

A. Singular ground-state occupation

Induced by a pump beam focused on an unstructured 2D region, singular ground-state condensation around 3.06 eV, $\lambda = 405.2$ nm, is observed. Figure 2 shows the Fourier plane images below [Fig. 2(a)] and above [Fig. 2(b)] the lasing threshold at RT. The evolution of the emission with increasing pump power is given in Fig. 3. The averaged threshold power amounts to $P_{thr}(RT) = 50\ \mu W$ which is equivalent to an energy of 5.87 nJ per pulse. This corresponds to an average power density of 78 mW/cm^2 or 9 μJ/cm^2 per pulse. Compared to recently published optical pumped InGaN VCSELs [24], this value is three orders of magnitude smaller. Assuming a

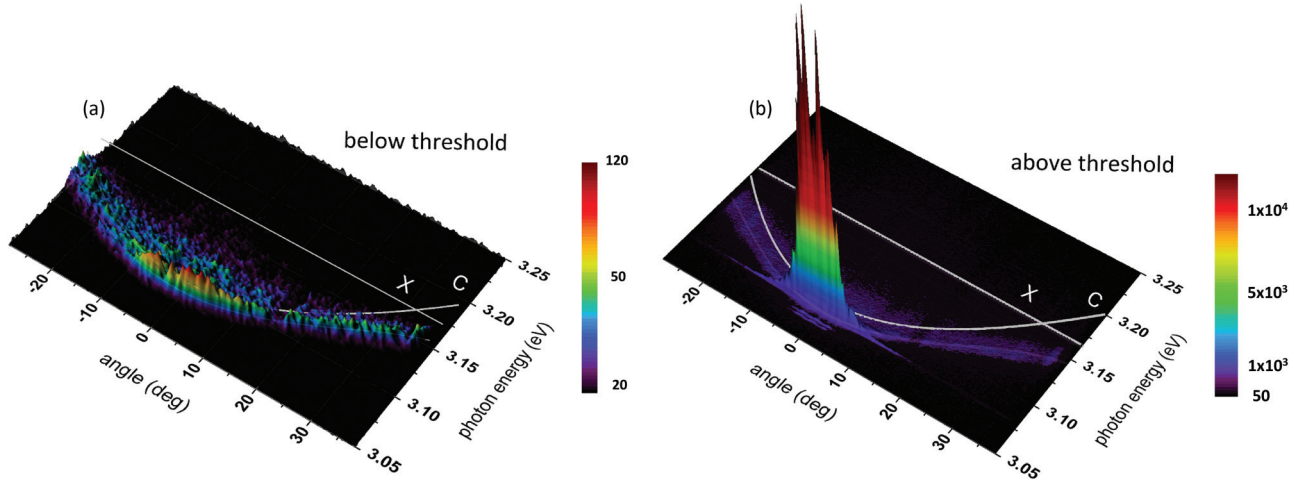

FIG. 2. Room-temperature far field (Fourier-plane) images of the single-state condensate emission (a) below and (b) above threshold pump power. X and C (white solid lines) mark the uncoupled excitonic energy and the pure cavity (photonic) mode, respectively. Scale bars refer to the color-coded emission intensity. Above threshold, the emission is dominated by a massive flat mode with narrowed linewidth.

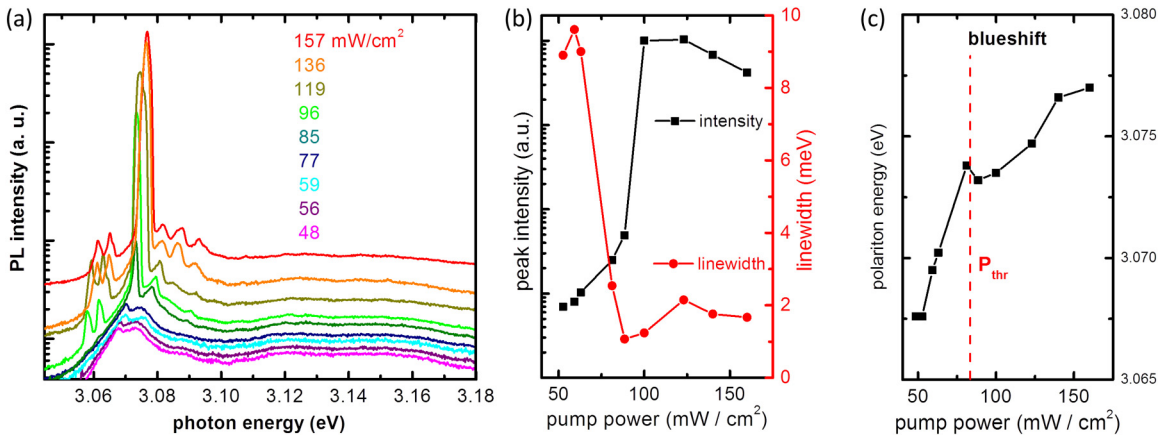

FIG. 3. PL measurements recorded at RT with different pump power: (a) the integrated PL for pump power sweep and (b) the peak intensity evolution. At threshold, abrupt spectral narrowing indicates the increase of temporal coherence and a nonlinear rise of the emission intensity, the signature of a transition into a collective quantum phase. The blueshift in (c) is nonlinear and can explained by the condensation behavior of interacting particles.

cavity mode for a refractive index of $n_c = 2.6$ [18] and the free exciton energy to be 3.168 eV, the application of a coupled oscillator model would lead to a detuning $\delta = -72$ meV and a Rabi splitting of $\Omega_{\mathrm{VRS}} = 55$ meV. The effective mass is $m^* = 3.4 \times 10^{-5} m_e$, with m_e being the free electron mass, resulting in an excitonic fraction around $X_{k=0} = 17\%$.

Unintentional confinement induced by the static disorder can additionally trigger condensation [25] because the increase of the number of quasiparticles being in the same eigenstate happens without the need for enhancing the overall exciton density [26,27]. Separate neighboring condensates fed by the same reservoir are considered to be linked in phase to each other, maintaining overall coherence [28].

1. Blueshift

The blueshift of the ground-state emission with increasing power is displayed in Fig. 3(c). The steep blueshift below threshold is due to the branch filling mainly into an excitonic reservoir at large k values. Once a coherent state is formed, the redshift relates to reservoir emptying by stimulated scattering (cooling) towards zero k triggered by the massive final state occupation. Because the lifetime of condensed exciton-photon composite bosons is shorter than in the reservoir, an overall decrease of the total number of excitons is the consequence. Above threshold, the rise of pump power again causes a blueshift with flattened slope. This can be described by increasing interparticle repulsion with increasing ground-state population while the reservoir occupancy remains small due to the fast decay of the condensate.

2. Carrier density and Mott transition

The exciton binding energy in typical strained thin layers of $In_{0.1}Ga_{0.9}N$ QWs is 30 meV [29]. The indication of the exciton Mott transition in InGaN QWs has been observed in recent reports [30,31] at 600 W/cm^2 and 1×10^{12}/cm^2 independent of T. We empirically deduce the carrier density by consideration of the incoming power from the pump laser and reflectivity and absorption of $R = 0.35$ and $A = 0.9$ through the top DBR, respectively [18]. Accounting for the lifetime of $\tau_x^{\mathrm{eff}} < 400$ ps the carrier density in two dimensions is given by 3.17×10^{10}/cm^2 in the case that carriers accumulate all in the same QW and the whole absorbed energy creates carriers without loss. Distributed among 15 QWs, the density does not exceeding 2.1×10^9/cm^2 which is orders of magnitude lower than the Mott -critical density around $n_{\mathrm{crit}} = 10^{12}$ [29,31,32].

The reported excitation densities at threshold for GaN polariton lasers are 30 W/cm^2 (bulk) [13] and 20 W/cm^2 (QWs) [14]. The lowest threshold at RT in GaN active medium was measured in a single nanowire with double dielectric DBRs with $P_{\mathrm{thr}} = 92$ nJ/cm^2 [15]. The reported second threshold in the latter device refers to conventional lasing marking the Mott transition at 250 μJ/cm^2. Here, one should mention that this low threshold is achieved by exciton confinement in a nanostructure and not in such a simple microtrap (pure photonic confinement) as reported here.

3. Oscillator strength

Here, the oscillator strength of the InGaN QW exciton is expected be higher in the final MC than in the as-grown active zone for several reasons. First, strain relaxation by the release of the membrane from the substrate leads to a considerable reduced quantum confined Stark effect (QCSE). The residual built-in electric field results in a polarization of spontaneous origin of around 115 kV/cm^3. In this case the oscillator strength of a QW exciton would have a value of $f_{\mathrm{osc}} = 2.4 \times 10^{-13}$ cm^{-2}, about twice the value when accounting for a usual strain-induced built-in field. Another situation in favor of strain relaxation could be the fact that microstructured layers allow a lateral relaxation (no large area layers). It is reported that mode confinement also enhances the oscillator strength [33]. Finally, the bonding process involves slow ramp heating up to 350°C for several hours, which has a certain annealing effect.

B. Multilevel condensate

When focusing the pump beam on the microwire spacer, the former 8/2 λ cavity locally switches to a 9/2 λ cavity.

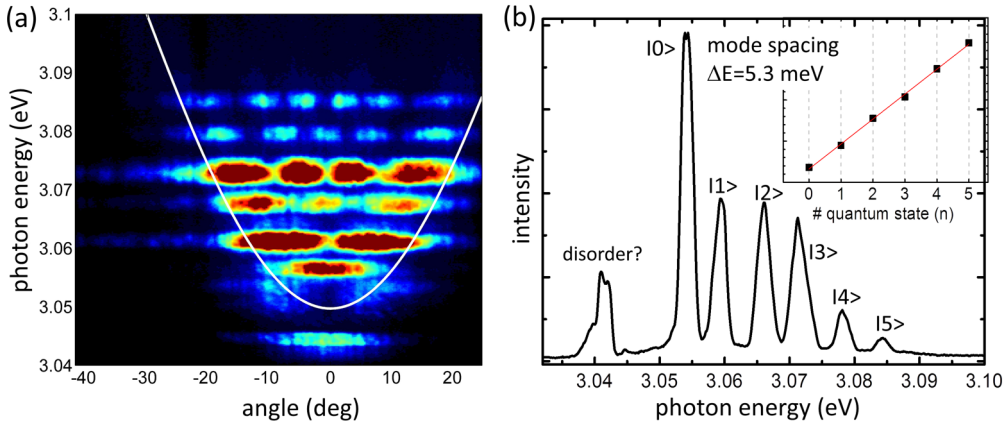

FIG. 4. Multilevel condensate inside the trap region. (a) Fourier image of emission pattern above threshold and with integrated variable pump powers at 200 K. The solid line sketches the parabolic potential shape. (b) Angle-integrated PL spectrum around 0° and (inlet) mode spacing plot showing the linear behavior of the excited quantized states. The additional weak emission might be caused by an additional trapping by disorder, which commonly perturbs only the ground state.

The spacer ΔL does not exactly match to $\lambda/2$ of the initial photon mode and leads to an energy offset. Here, the photon mode is a bit lower in energy resulting in a larger negative detuning of $\delta \approx -90$ meV and therefore higher photonic fraction. The excitonic fraction inside the wires is decreased to $X_{k=0} = 6\%$.

The measured energy-momentum spectral function of the trap region in Figs. 4(a) and 4(b) displays the wave function observable for 200 K and the emission profile at $k = 0$, respectively. Narrow linewidth peaks equally spaced in energy with a constant separation of 5.3 meV for 200 K and 5.5 meV for RT [18] and a linear behavior of excited states characterize the emission. The small deviation in the spacing can be related to the slight variation in the wire size due to temperature expansion. The thermal de Broglie wavelength in the unstructured region λ_{dB} is 680 nm at RT and about 1 μm at 200 K.

The set of discrete levels shifts to lower energy with increasing temperature by 0.3 meV/K which is lower than the pure band gap narrowing of 0.5–1.2 meV/K, while the spacing stays equal. Pure photonic modes would not change energy with temperature (only by the small n dependence) while the mode interval only depends on the structural trap dimension. This can be taken as an additional proof for the excitonic fraction of the photonic condensate.

The pump spot exposes the microwire with a Gaussian intensity distribution [18]. Inside the spacer this pictures a Gauss profile with a high density gradient inside the microwire. While the Gauss profile acts as a smooth antitrapping potential, the wire edges can be seen as high potential walls that cause back-reflection. The observation of 1D standing waves inside the microwire implies the formation of an oscillating quantum fluid over a distance of 6 μm. Although the natural disorder landscape likely causes several localized condensates to form in the lower potential levels [25], they are considered to be linked in phase and therefore mutually coherent [28], maintaining the order over at least the range of the wire. Moreover, it was shown theoretically that the flowing conditions are not altered by the separation [28]. However, at higher temperature or increased pump density, localized fluids can escape the traps at the nanoscale, causing an overlap of neighboring islands and starting to merge into a single condensate.

The driving force for the dynamics in the condensate is considered to be caused by the Gauss-distributed spatial dependence of the pump beam. The strong gradient in the particle density (nonlinearity) induces pronounced outward ballistic acceleration [34] which is back-reflected from the wire edges and therefore an oscillation of wave packets is established. The pump decay dynamics of a nonequilibrium and inhomogeneous quantum-degenerate state of interacting bosons induce shape changes, and stationary flow is possible. The polariton field is coupled to an incoherent active excitonic reservoir [only phase-matched excitonic(-polariton) states can contribute to stimulated scattering] which feeds directly the condensate population. Repulsive interaction with the condensate mainly arises from this part of the reservoir together with the inactive background carriers in addition to weak polariton-polariton interaction [35].

The presence of repelling (quasi)particles physically explains condensation far from zero k, while the noncondensed structureless thermal reservoir cloud exists outside the trap [36]. The general mechanism was also described in (Al)GaAs-based MCs in pillars [37] or under optical treatment [38] at low temperature, and the results are qualitatively similar. Here, the essential difference is that it is demonstrated in structural rather than optically created traps and by its sophisticated operation at RT and visible wavelength with a lower threshold power.

Real-space images were taken simultaneously in order to display the spatial distribution of the condensate wave-function amplitude and also show the given geometry as can be seen in Fig. 5.

Remarkably, it is possible to create emission from specific orbitals separately. The controlled occupation is managed by a slight variation of pump power. This possibility was theoretically explained for 1D microwires [39] where the rate of energy relaxation between two modes is described by an increasing function of their energy difference and a gain mechanism depending on the balance between loss and incoming population. The relaxation rate in turn is proportional to the condensed polariton density in a level and the energy

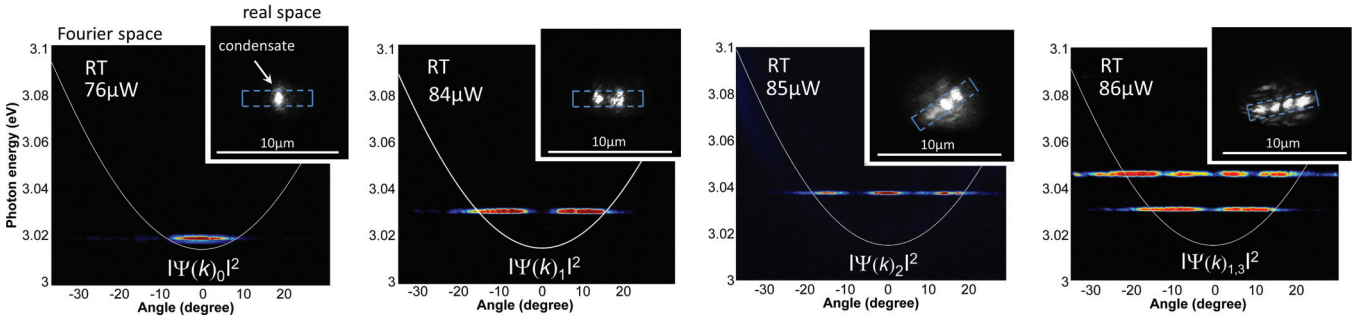

FIG. 5. Fourier images of the separate excitations and corresponding real-space pattern (right upper inlet) at RT. Discrete quantization levels with a regular angular pattern indicate stationary wave functions in higher orbitals starting with the single ground state, the first and second excited state, and the coexistence of two odd orbital states—the first and the third. The selection of orbitals is managed by pump power variation. The white parabolic line marks an appropriate harmonic potential shape. The blue dotted rectangular box is drawn into the real-space images to mark the spacer shape and orientation for convenience. Real- and Fourier-space images for a certain pump power are simultaneously recorded.

difference to the next. Furthermore, relaxation is more effective near the wire edges. Here, the wire is shorter than the long-range order of the condensate, so that relaxation always happens near both ends of the wire.

A harmonic oscillator model to handle the situation seems most adaptive since the observed pattern suggests a quadratic potential shape [38], which is invariant to Fourier transformation from momentum to real space. Accounting for nonlinear drive and dissipation-process-induced damping, a model for a nonlinear harmonic oscillator suitable for a quantum condensate in a 1D harmonic trap is used. The 1D problem is applied along the axial direction of the microwire spacer (x), which is the direction of weak confinement. Simultaneously, the motion in the y direction is frozen out (strong lateral confinement). The macroscopic wave function of a condensate is usually described by the 2D Gross-Pitaevskii equation (GPE) in the time domain containing the interparticle interaction parameter λ, the effective mass m_*, and the axial-longitudinal trap potential $V(\vec{r}) = U_x + U_y$:

$$i\hbar\delta_t\Psi = \left(-\frac{\hbar^2}{2m_*}\Delta + V(\vec{r}) + \lambda|\Psi|^2\right)\Psi.$$

For 1D motion of the condensate within the microwire spacer a parabolic axial trap potential $U_x(x) = 1/2m\omega_{0y}x^2$ is applied, while the transverse direction of the cavity width is restricted to much smaller length than that of the harmonic oscillator. The stationary solutions of the effective 1D GPE are [40]

$$\Psi(\vec{r}t) = \sqrt{N}\phi_x(x,t)e^{-iE_yt/\hbar}\phi_y(y) \quad (1)$$

with ϕ_y being the longitudinal wave function with eigenenergies $E_y = \hbar\omega_{ny}$ with

$$\omega_{ny} = \frac{\hbar}{2m_*}\left(\frac{n_y\pi}{L_y}\right)^2 \quad (2)$$

being the trap frequency for the microwire cavity depth L_y. For the axial direction the GPE then equals

$$i\hbar\delta_t\phi_x = \left(\frac{p_x^2}{2m_*} + U_x + g_1|\phi_x|^2\right)\phi_x, \quad (3)$$

with $g_1 = 3\lambda N/(2L_y)$ being the effective interaction constant. The system is expected to be in a regime of rather low density and medium repulsive interaction strength between the quasiparticles (Gaussian density profile) [34] so that the perturbation method holds. Details and exact solutions of the simulation of the 1D GPE and spectra of states can be found elsewhere [40]. It should be mentioned that here, the equilibrium GPE is used, although the system is obviously strongly out of equilibrium. However, the spatial pattern in the laser emission is resembled in a qualitatively satisfying way while keeping the model very simple and by explicitly including the 1D nature of a harmonic oscillator. Another relevant and advanced model calculation additionally considering the nonequilibrium nature of the condensate is reported in the work of Wouters *et al.* [28].

IV. CONCLUSION AND OUTLOOK

In summary, the direct observation of singular and discrete multilevel polariton condensates with a high photonic fraction in an InGaN microcavity is reported. The condensation threshold density is orders of magnitude smaller than in recent GaN VCSELs and lower than in most other polariton lasers. It is shown that the system resides significantly below the Mott critical density. The close similarity to the well-established VCSEL design, the use of mainly standard processing and growth techniques, and the RT operation at visible wavelength represent an important building block towards simple integration into practical applications. Simple 1D microwire spacer traps offer strong confinement in two directions and weak confinement along one dimension, creating a 1D quantum harmonic oscillator emulating a macroscopic quantum emitter with equally spaced discrete states in photonic orbitals. Single-mode lasing with a specific energy and angular momentum can be optically controlled by pump power variation. This multistability system holds more attractive features than a single-mode laser. For example, in a recent theoretic work [41], the implementation of this 1D polariton harmonic oscillator as a NOR gate in a Boolean logic system is described which, applied to the InGaN MC, would enable polariton optical computing and logic gate operations at room temperature. From a fundamental view this work introduces room-temperature

photonic fluids as a coherent light source utilizing weakly interacting Bose gases [1].

In a further outlook, interacting highly photonic quasiparticles hold attractive features and should motivate future investigations towards nonseparability of emitted correlated pairs, photon-blockade effects, 1D Tonks-Girardeau gases [42], photonic vortices, and cavity electromagnetically induced transparency (EIT).

ACKNOWLEDGMENTS

The author would like to thank Jean-François Carlin for the excellent MOVPE growth, Alexey Kavokin for his constant support and valuable comments, and Nicolas Grandjean for guidance through the project (which was funded by EU-project Grant No. FP7-235114).

[1] I. Carusotto and C. Ciuti, Rev. Mod. Phys. **85**, 299 (2013).
[2] J. Klaers, J. Schmitt, F. Vewinger, and M. Weitz, Nature (London) **468**, 545 (2010).
[3] S. I. Pekar, Zh. Eksp. Teor. Fiz. **33**, 1022 (1957) [Sov. Phys. JETP **9**, 314 (1959)].
[4] J. J. Hopfield, Phys. Rev. **112**, 1555 (1958).
[5] M. Cobet, C. Cobet, M. R. Wagner, N. Esser, C. Thomsen, and A. Hoffmann, Appl. Phys. Lett. **96**, 031904 (2010).
[6] A. Imamoğlu, R. J. Ram, S. Pau, and Y. Yamamoto, Phys. Rev. A **53**, 4250 (1996).
[7] J. Kasprzak, M. Richard, S. Kundermann, A. Baas, P. Jeambrun, J. M. J. Keeling, F. M. Marchetti, M. H. Szymanska, R. Andre, J. L. Staehli, V. Savona, P. B. Littlewood, B. Deveaud, and Le Si Dang, Nature (London) **443**, 409 (2006).
[8] Benoît Deveaud-Plédran, J. Opt. Soc. Am. B **29**, A138 (2012).
[9] D. Racine and P. R. Eastham, Phys. Rev. B **90**, 085308 (2014).
[10] M. A. Cazalilla, R. Citro, T. Giamarchi, E. Orignac, and M. Rigol, Rev. Mod. Phys. **83**, 1405 (2011).
[11] M. Assmann, J.-S. Tempel, F. Veit, M. Bayer, A. Rahimi-Iman, A. Löffler, S. Höfling, S. Reitzenstein, L. Worschech, and A. Forchel, Proc. Natl. Acad. Sci. USA **108**, 1804 (2010).
[12] T. Guillet, M. Mexis, J. Levrat, G. Rossbach, C. Brimont, T. Bretagnon, B. Gil, R. Butté, N. Grandjean, L. Orosz, F. Réveret, J. Leymarie, J. Zúñiga-Pérez, M. Leroux, F. Semond, and S. Bouchoule, Appl. Phys. Lett. **99**, 161104 (2011).
[13] S. Christopoulos, G. Baldassarri Höger von Högersthal, A. J. D. Grundy, P. G. Lagoudakis, A. V. Kavokin, and J. J. Baumberg, G. Christmann, R. Butté, E. Feltin, J.-F. Carlin, and N. Grandjean, Phys. Rev. Lett. **98**, 126405 (2007).
[14] G. Christmann, R. Butté, E. Feltin, J.-F. Carlin, and N. Grandjean, Appl. Phys. Lett. **93**, 051102 (2008).
[15] A. Das, J. Heo, M. Jankowski, W. Guo, L. Zhang, H. Deng, and P. Bhattacharya, Phys. Rev. Lett. **107**, 066405 (2011).
[16] P. Bhattacharya, T. Frost, S. Deshpande, M. Z. Baten, A. Hazari, and A. Das, Phys. Rev. Lett. **112**, 236802 (2014).
[17] I. Iorsh, M. Glauser, G. Rossbach, J. Levrat, M. Cobet, R. Butte, N. Grandjean, M. A. Kaliteevski, R. A. Abram, and A. V. Kavokin, Phys. Rev. B **86**, 125308 (2012).
[18] See Supplemental Material at http://link.aps.org/supplemental/10.1103/PhysRevB.94.075302 for details.
[19] J. Dorsaz, H.-J. Bühlmann, J.-F. Carlin, N. Grandjean, and M. Ilegems, Appl. Phys. Lett. **87**, 072102 (2005).
[20] A. Altoukhov, J. Levrat, E. Feltin, J.-F. Carlin, A. Castiglia, R. Butté, and N. Grandjean, Appl. Phys. Lett. **95**, 191102 (2009).
[21] R. Balili, V. Hartwell, D. Snoke, L. Pfeiffer, and K. West, Science **316**, 1007 (2007).
[22] F. Ding, T. Stöferle, L. Mai, A. Knoll, and R. F. Mahrt, Phys. Rev. B **87**, 161116(R) (2013).
[23] A. V. Kavokin, A. S. Sheremet, I. A. Shelykh, P. G. Lagoudakis, and Y. G. Rubo, Sci. Rep. **5**, 12020 (2015).
[24] W. Liu, S. Chen, X. Hu, Z. Liu, J. Zhang, L. Ying, X. Lv, H. Akiyama, Z. Cai, and B. Zhang, IEEE Photonics Technol. Lett. **25**, 1041 (2013).
[25] G. Malpuech, D. D. Solnyshkov, H. Ouerdane, M. M. Glazov, and I. Shelykh, Phys. Rev. Lett. **98**, 206402 (2007).
[26] M. Richard, J. Kasprzak, R. André, R. Romestain, Le Si Dang, G. Malpuech, and A. Kavokin, Phys. Rev. B **72**, 201301(R) (2005).
[27] P. Cristofolini, A. Dreismann, G. Christmann, G. Franchetti, N. G. Berloff, P. Tsotsis, Z. Hatzopoulos, P. G. Savvidis, and J. J. Baumberg, Phys. Rev. Lett. **110**, 186403 (2013).
[28] Michiel Wouters, Iacopo Carusotto, and Cristiano Ciuti, Phys. Rev. B **77**, 115340 (2008).
[29] *III-Nitride Semiconductors and their Modern Devices*, edited by Bernard Gil (Oxford University Press, New York, 2013).
[30] M. Glauser, C. Mounir, G. Rossbach, E. Feltin, J.-F. Carlin, R. Butté, and N. Grandjean, J. Appl. Phys. **115**, 233511 (2014).
[31] G. Rossbach, J. Levrat, G. Jacopin, M. Shahmohammadi, J. F. Carlin, J.-D. Ganiére, R. Butté, B. Deveaud, and N. Grandjean, Phys. Rev. B **90**, 201308 (2014).
[32] P. Bigenwald, A. Kavokin, B. Gil, and P. Lefebvre, Phys. Rev. B **61**, 15621 (2000).
[33] L. Zhang, T. A. Hill, H. Deng, L.-K. Lee, C.-H. Teng, and P.-C. Ku, Appl. Phys. Lett. **104**, 051116 (2014).
[34] Y. N. Fernández, M. I. Vasilevskiy, C. Trallero-Giner, and A. Kavokin, Phys. Rev. B **87**, 195441 (2013).
[35] J. Schmutzler, P. Lewandowski, M. Assmann, D. Niemietz, S. Schumacher, M. Kamp, C. Schneider, S. Höfling, and M. Bayer, Phys. Rev. B **91**, 195308 (2015).
[36] S. Utsonumiya, L. Tian, G. Roumpos, C. W. Lai, N. Kumada, T. Fujisawa, M. Kuwata-Gonokamis, A. Löffler, S. Höfling, A. Forchel, and Y. Yamamoto, Nat. Phys. **4**, 700 (2008).
[37] L. Ferrier, E. Wertz, R. Johne, D. D. Solnyshkov, P. Senellart, I. Sagnes, A. Lemaitre, G. Malpuech, and J. Bloch, Phys. Rev. Lett. **106**, 126401 (2011).
[38] G. Tosi, G. Christmann, N. G. Berloff, P. Tsotsis, T. Gao, Z. Hatzopoulos, P. G. Savvidis, and J. J. Baumberg, Nat. Phys. **8**, 190 (2012).
[39] M. Wouters, T. C. H. Liew, and V. Savona, Phys. Rev. B **82**, 245315 (2010).
[40] C. Trallero-Giner, M. V. Durnev, Y. N. Fernández, M. I. Vasilevskiy, V. López-Richard, and A. Kavokin, Phys. Rev. B **89**, 205317 (2014).
[41] F. Pinsker and T. J. Alexander, Proc. R. Soc. London A **471**, 20150210 (2015).
[42] T. Kinoshita, T. Wenger, and D. S. Weiss, Science **305**, 1125 (2004).